Smart Materials and Structures

Thermal behavior of a metal embedded fiber Bragg grating sensor

To cite this article: Xiao Chun Li *et al* 2001 *Smart Mater. Struct.* **10** 575

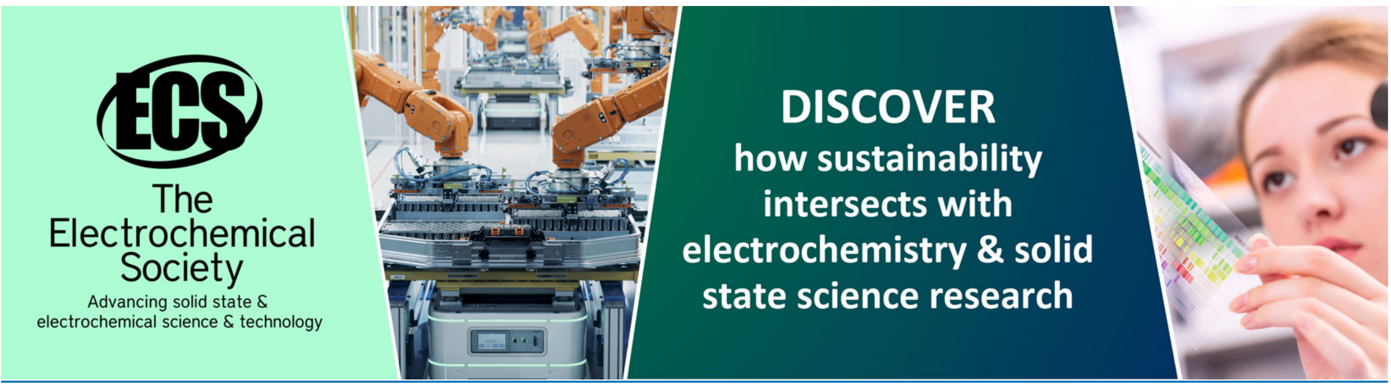

Smart Mater. Struct. **10** (2001) 575–579 PII: S0964-1726(01)22819-5

Thermal behavior of a metal embedded fiber Bragg grating sensor

Xiao Chun Li[1], Fritz Prinz[1] and John Seim[2]

[1] Rapid Prototyping Laboratory, Building 530 Room 226, Stanford University, Stanford, CA94305, USA
[2] Blue Road Research, 2555 N E 205th Avenue, Fairview, Oregon 97024, USA

Received 23 November 1999, in final form 29 August 2000
Published 18 July 2001
Online at stacks.iop.org/SMS/10/575

Abstract
With embedded sensors it is possible to monitor structural parameters at critical locations which are not accessible to ordinary sensors. Recently, the fiber optic sensor has emerged as a promising technology to be integrated with structures. The embedding of fiber optic sensors into composites and some metals, especially those with low melting points, have been reported. However, all reported embedding techniques so far are either complicated or it is difficult to achieve coherent bonding with low residue stresses. Thus, it is of interest to pursue some economical ways to embed fiber optic sensors into metallic structures with low residue stresses. In this work, a new technique is proposed for embedding a fiber optic sensor into metallic structures, such as nickel, with minimized residue stress. Fiber Bragg grating (FBG) sensors have been embedded into nickel structures. The thermal performance of such an embedded FBG sensor is studied. Higher temperature sensitivity is demonstrated for the embedded FBG sensors. For temperature measurements, the embedded FBG sensor yields an accuracy of about 2 °C. Under rapid temperature changes, it is found that thermal stresses due to the temperature gradient in the metallic structures would be the main cause for errors.

(Some figures in this article are in colour only in the electronic version)

1. Introduction

Embedded sensors within structural materials add intelligence into structures and enable real-time monitoring at some critical locations not accessible to ordinary sensors, which must be attached to the surface. The embedded sensor is also protected from damage and isolated from extraneous environmental effects by the structure itself. In some cases, this can be a huge advantage. Recently, fiber optic sensors and communication links have emerged as a promising technology to be integrated with structures, which is termed fiber optic smart structures. They allow critical parameters of materials and structures to be sensed while offering low weight, immunity to electromagnetic interference, the ability to be shielded from hostile environments, and extremely high bandwidth capability [1]. A network of embedded fiber optic sensors can allow a structure to monitor its integrity or health during manufacturing and service. Moreover, these sensors could replace many of the functions traditionally performed by human visual inspection and could provide real-time feedback in the event of structure failure.

Fiber optic sensor embedding has been investigated intensively for composite structures [1, 2]. However, only a few papers have demonstrated techniques with which to embed the fiber optic sensor in metal parts [2–6]. Taylor and Lee and co-workers have embedded optical fibers and Fabry–Pérot Interferometers into aluminum (melting point 660 °C) by casting in a graphite mold [2, 3]. In order to increase the temperature sensitivity of the fiber Bragg grating (FBG) sensor, Lin *et al* [4] used lead cladding to enhance the sensitivity. The metal cladding process produced large residue stress. Baldini *et al* [5] used gold coatings for placing single-mode fibers into titanium matrix composites by arc spraying. All these embedding techniques are either complicated or it is difficult to achieve coherent bonding with low residue stresses. Thus, it is of interest to pursue some economical ways to embed fiber optic sensors into metallic structures with low residue stresses. In this work, the authors propose a new technique for

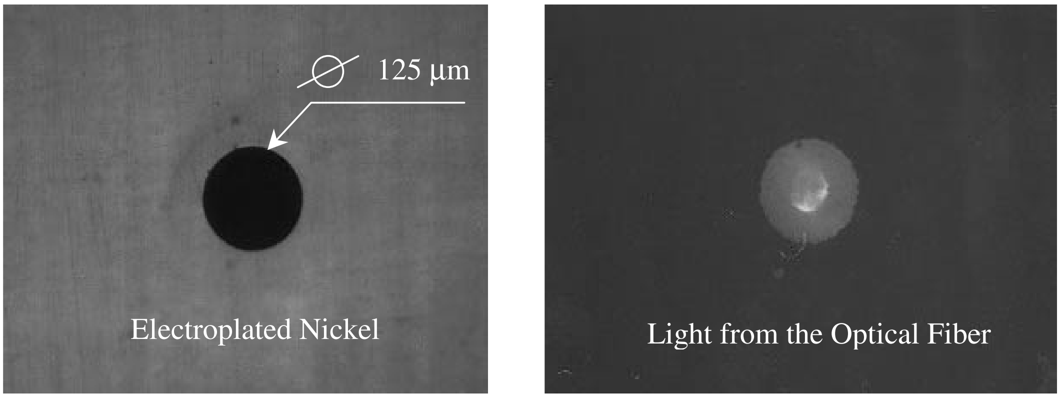

Figure 1. Cross section of embedded optical fiber.

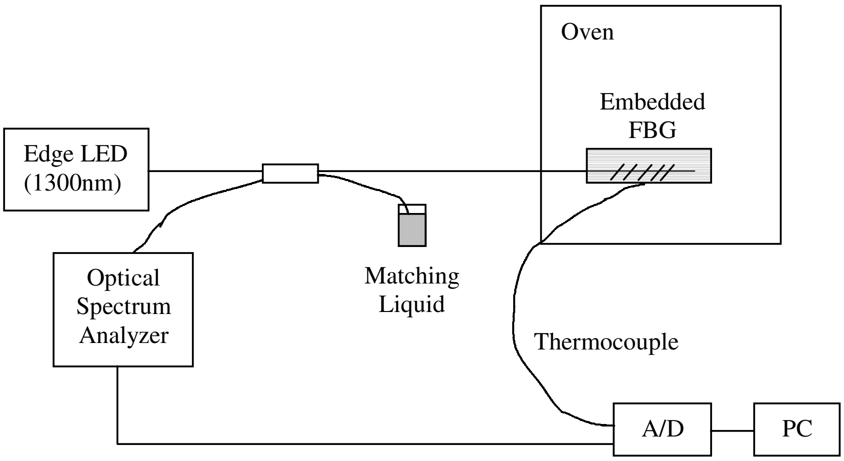

Figure 2. Experimental setup for temperature measurements.

embedding fiber optic sensors into metallic structures, such as nickel, with minimized residue stress. Since FBG sensors have been identified as one of the most promising sensor candidates for smart structure applications [1], the feasibility of fabricating a metal embedded FBG sensor is investigated. The thermal performance of such embedded FBG sensors is reported.

2. Theory for FBG

The FBG is compact, simple and can be demodulated in a wavelength-coding manner. When the FBG is expanded or compressed, it changes the grating spectral response. The temperature dependence of the Bragg wavelength is related to the temperature dependence of the index of refraction n_0 and the Bragg grating period d_0 through the equation

$$\lambda_0 = 2d_0n_0.$$

By differentiating the equation, the Bragg wavelength shift $\Delta\lambda$ is given by

$$\Delta\lambda = 2\Delta d_0n_0 + 2d_0\Delta n_0$$

which leads to

$$\frac{\Delta\lambda}{\Delta T} = \lambda_0\left(\alpha + \frac{1}{n_0}\frac{\mathrm{d}n_0}{\mathrm{d}T}\right)$$

where α is the coefficient of thermal expansion (CTE). For fused silica at room temperature, α is approximately $0.55 \times 10^{-6}\,^{\circ}\mathrm{C}^{-1}$, n_0 is 1.4469, and $\mathrm{d}n/\mathrm{d}T$ is approximately $9.1 \times 10^{-6}\,^{\circ}\mathrm{C}^{-1}$ at room temperature [6]. From the theory, the temperature sensitivity of a bare FBG is about $0.008\,89$ nm $^{\circ}\mathrm{C}^{-1}$. If the FBG sensor is embedded in a bulk metallic structure, the value of α should be replaced with that of the metallic structure. Higher α yields higher temperature sensitivity for the sensor [4].

3. Embedding techniques

The problem of developing a metal embedded fiber optic sensor (MEFOS) arises from the high melting point of metals, such as steel, nickel, iron and titanium etc, at which a silica-based fiber would be damaged during material processing if there was no protection. To solve this problem, a new technique has been developed in our laboratory involving low-temperature processes, magnetron sputtering and electroplating. For the first step, the optical fiber is sputter coated with a thin titanium film (1 μm) to enhance the adhesion with the optical fiber. Then a thin nickel film (about 2 μm) is sputter coated over the thin titanium film. Afterwards, the optical fiber can be placed in a designated path (straight or curved), that can be created manually or patterned by LIGA/MEMS techniques. Then the

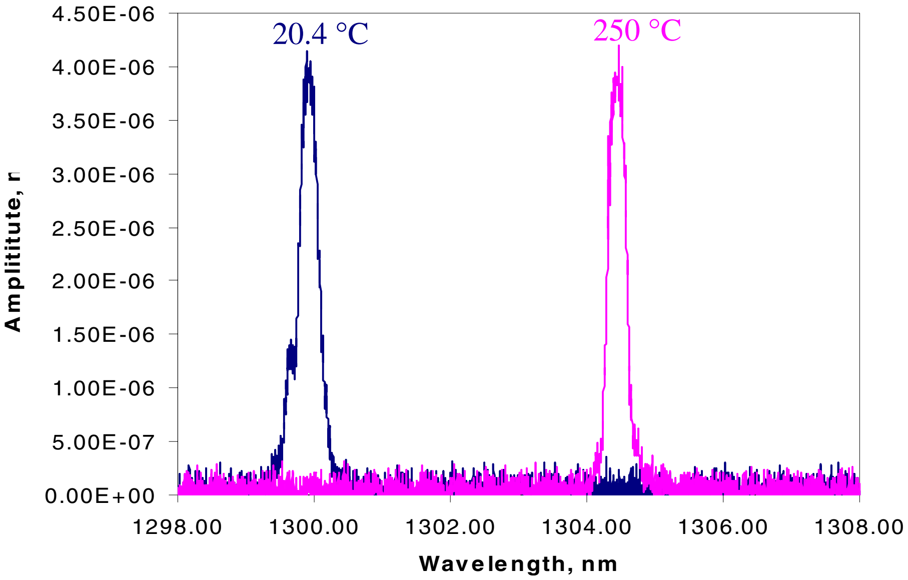

Figure 3. Typical spectral response of an embedded FBG with different temperatures.

fiber is electroplated up to about a 0.25–1 mm thick nickel layer. To ensure low residue stresses from the electroplating process, a Barrett SN solution (nickel sulfamate) plating bath is used. The temperature of the plating bath is controlled at 49 °C. A dc power supply is applied to control the current density. For the first hour of plating, the current density is set at 0.215 mA mm^{-2}. Afterwards, the current density is raised to 0.646 mA mm^{-2}.

The optical fiber can be continuously electroplated into a thicker nickel layer or embedded into the other metallic structures by high-temperature processing (casting, welding, arc spraying, etc). In some early experiments, optical fibers were embedded into stainless steel structures by laser cladding. The optical fiber diameter used was 125 μm and thus the fiber optic sensor provides very little intrusiveness to the metallic structure. Those techniques employed in the embedding process also ensure good integrity for the metal embedded optical fiber, as shown in figure 1.

4. Thermal performance of embedded FBG

Single axis fiber gratings in a polyamide coated 125 μm diameter single-mode fiber for operation at 1300 nm were provided by Blue Road Research, OR. The specifications include a reflected wavelength of 1300 ± 0.3 nm, 5 mm grating period, and an annealing temperature of 300 °C. For embedding into metal, the polyamide coating was carefully burned off and then the embedding procedure as described above was applied. For simplicity, the tested sensors were only electroplated to their final sizes. The dimensions of the samples were 50 mm × 10 mm × 2 mm with a Bragg grating embedded in the center.

4.1. Experimental setup and procedures

To characterize the thermal behavior of the metal embedded FBG sensor, the experimental scheme was setup as shown in figure 2. A broadband ELED (edge light emitting diode) light source with a central wavelength of 1300 nm was connected to a 3 dB beam splitter. Half of the light was guided out to the metal embedded Bragg grating sensor, which was put inside an oven for temperature control. Another half of the light was guided by the single-mode fiber to an index matching liquid. The FBG sensor acts as a temperature transducer and reflects a very small spectral peak back towards the light source but allows most of the optical power to pass through. Through the beam splitter, half of the reflected light is captured with an Ando 6315A optical spectrum analyzer with an accuracy of ±0.02 nm. To verify the oven temperature, a JK type thermal couple, with a Fluke 80TK thermocouple module, was attached to the sample near the Bragg grating position. The signal from the optical spectrum analyzer and thermocouple were collected by a National Instruments AI-16XE-50 DAQ Card, which was installed in a Dell Notebook PC.

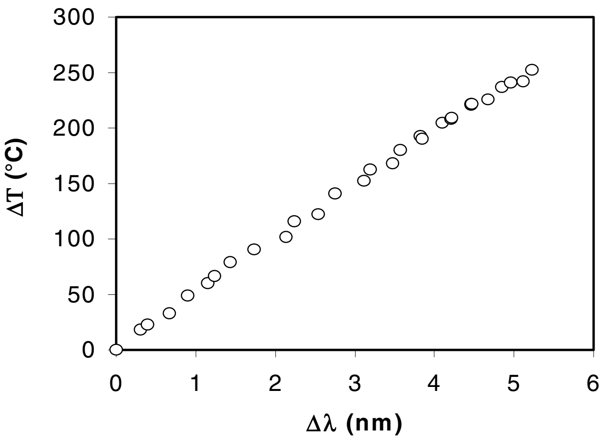

Figure 4. Temperature change versus wavelength shift.

At first, the static temperature dependence of the embedded FBG was characterized. The sample was subjected to different testing temperatures from 20 °C to about 300 °C.

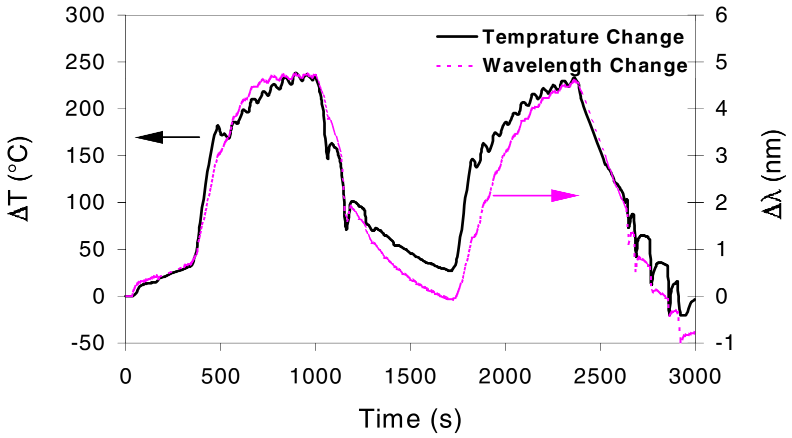

Figure 5. Wavelength shifts under cyclic temperature changes.

At each testing temperature, the specimen was held for approximately 5 min to achieve thermal equilibrium. The wavelength shifts and temperature changes were recorded for approximately 2 min and averaged.

The experiments were designed to investigate the response to thermal cycles. The specimen was subjected to two thermal cycles from 20 °C to 260 °C. To increase the cooling rate, some coolant was sprayed on the surface of the specimen. The temperature and wavelength were recorded simultaneously.

4.2. Results and discussion

Figure 3 presents the spectral response of the embedded FBG to the static thermal load. Two typical values of the spectral response for two different temperatures are presented. At a room temperature of 20.4 °C, which was measured by the thermocouple, the peak wavelength of the reflected light for the embedded FBG was about 1299.94 nm. This wavelength was almost exactly equal to a bare FBG at room temperature. Thus, the low-temperature embedding processes, sputtering and electroplating, produce almost no residual stress in the embedded FBG sensors. This is an advantage over other reported embedding processes [2–4]. At the temperature of 250 °C, the peak wavelength of the reflected light was about 1304.5 nm. In a span of about 230 °C, the embedded FBG wavelength was shifted by about 4.65 nm. More information is shown in figure 4, which is presented as the temperature change versus wavelength shift. The wavelength shift is quite linear to the temperature change. The embedded FBG sensor yields an accuracy of about 2 °C with the experimental setup. The temperature sensitivity of the embedded FBG is about 0.021 nm °C^{-1}. The sensitivity is more than twice as high as that of bare FBG. Theoretical temperature sensitivity can be obtained by the equation

$$\frac{\Delta\lambda}{\Delta T} = \lambda_0 \left(\alpha + \frac{1}{n_0}\frac{\mathrm{d}n_0}{\mathrm{d}T}\right).$$

With the assumptions of the constant CTE of nickel, 12 $\mu\varepsilon$ °C^{-1}, and perfect bonding between the optical fiber and bulk nickel, the temperature sensitivity was calculated to be about 0.0237 nm °C^{-1}. The theoretical sensitivity was about 10% larger than that from experiments. The difference might be due to the selected values of n_0, 1.4469, $\mathrm{d}n_0/\mathrm{d}T$, 9.1×10^{-6} °C^{-1}, and a constant CTE of nickel, 12 $\mu\varepsilon$ °C^{-1}. It is especially difficult to obtain an accurate value of $\mathrm{d}n/\mathrm{d}T$ since manufacturers do not provide this data for the FBGs. An error analysis is necessary to determine the effects of the three different terms on the temperature sensitivity:

$$\mathrm{d}\left(\frac{\Delta\lambda}{\Delta T}\right) = \lambda_0 \left[\mathrm{d}\alpha + \mathrm{d}\left(\frac{1}{n_0}\frac{\mathrm{d}n_0}{\mathrm{d}T}\right)\right]$$

which can be converted to

$$\mathrm{d}\left(\frac{\Delta\lambda}{\Delta T}\right) = \lambda_0\alpha\frac{\mathrm{d}\alpha}{\alpha} + \lambda_0\frac{1}{n_0}\frac{\mathrm{d}n_0}{\mathrm{d}T}\left(\frac{\mathrm{d}\,(\mathrm{d}n_0/\mathrm{d}T)}{\mathrm{d}n_0/\mathrm{d}T} - \frac{\mathrm{d}n_0}{n_0}\right)$$

that is (with $\lambda = 1299.4$ nm, $\alpha = 12 \times 10^{-6}$, $n_0 = 1.4469$, and $\mathrm{d}n_0/\mathrm{d}T = 9.1 \times 10^{-6}$)

$$\mathrm{d}\left(\frac{\Delta\lambda}{\Delta T}\right) = 0.015\,593\frac{\mathrm{d}\alpha}{\alpha} + 0.008\,172\frac{\mathrm{d}\,(\mathrm{d}n_0/\mathrm{d}T)}{\mathrm{d}n_0/\mathrm{d}T} - 0.008\,172\frac{\mathrm{d}n_0}{n_0}.$$

As shown in the above analysis, an error in the CTE of nickel, $\mathrm{d}\alpha/\alpha$, will result in an error of the temperature sensitivity nearly twice as large as the one induced by an error in $\mathrm{d}(\mathrm{d}n_0/\mathrm{d}T)/(\mathrm{d}n_0/\mathrm{d}T)$ or $\mathrm{d}n_0/n_0$. Thus, by applying more accurate values of α, n_0 and $\mathrm{d}n_0/\mathrm{d}T$, the theoretical value of the temperature sensitivity might be closer to that from experiments.

The experimental results under thermal cycles are presented in figure 5. The specimen was subjected to two thermal cycles from 20 °C to 260 °C. The sample was initially heated up from room temperature. At the time of 500 s, the thermocouple indicates a slight surge at a temperature change of 175 °C while the wavelength shift of FBG does not follow well. This might due to the low sampling frequency of the optical spectrum analyzer. From room temperature to about 260 °C during about the first 1000 s, the temperature sensitivity matches that of the static thermal load very well, about 0.021 nm °C^{-1}. At 1050 s, some coolant is sprayed at the surface of the sample to increase the cooling rate. A sudden temperature drop appears and the temperature rapidly increases again. With spraying the coolant again, the temperature curve experiences another sudden drop while the wavelength curve is much smoother. For a temperature change down to 26 °C, the wavelength shift drops to almost zero. The wavelength shift should be about 0.52 nm, which corresponds to the 26 °C temperature change if the temperature sensitivity of 0.021 nm °C^{-1} is applied. The difference is possibly induced by the thermal stress due to the large temperature gradient at the moment when coolant is sprayed on the top surface of the sample. At the second thermal cycle, the wavelength shift obviously lags behind the temperature change until the temperature change reaches the peak at about 260 °C, where the temperature sensitivity is back to about 0.021 nm °C^{-1} again. It is possible that the sample experiences a process like annealing when the sample is heated for 10 min. After the second peak of temperature changes, the temperature sensitivity matches with 0.021 nm °C^{-1} very well until the coolant is applied again. The temperature gradient induces compressive residue stress, which shifts the wavelength down by almost 1 nm, when the sample is cooled to room temperature. Thus, the temperature gradient applied to the embedded FBG sensor can cause errors if it is used to measure temperatures. It will be advantageous if a new design of an embedded FBG sensor can separate the effect of temperature from that of stress.

5. Conclusions

A new technique is being developed, which involves low-temperature processes, magnetron sputtering and electroplating. The optical fiber can be continuously electroplated into a thicker metallic layer or embedded into other metallic structures by high-temperature processing (casting, welding, arc spraying, etc). Since the optical fiber diameter is 125 μm, the fiber optic sensor is unobtrusive. The techniques employed in the embedding process also ensure good integrity for the metal embedded optical fiber. Furthermore, experimental results show that the new technique can be used to embed fiber optic sensors into nickel structures with little residual stress.

FBG sensors have been embedded into nickel structures and their thermal performance has been studied. For the embedded FBG sensors, approximately 100% higher temperature sensitivity is demonstrated than that of bare FBG sensors. For temperature measurements, the embedded FBG sensor yields an accuracy of about 2 °C. However, it is found that thermal stresses due to the large temperature gradient, if there is any, in the metallic structures would be the main cause for errors if the embedded sensors are under rapid thermal cycles.

Acknowledgment

The authors would like to gratefully acknowledge the support of the Office of Naval Research (contract no N00014-96-1-0354-P00002).

References

[1] Udd E 1995 *Fiber Optic Smart Structures* (New York: Wiley)
[2] Taylor H F and Lee C E 1993 Sensing applications of fiber Fabry–Pérot interferometers embedded in composites and in metals *Experiments in Smart Materials and Structures* AMD-vol 181 (New York: ASME) p 47
[3] Lee C E, Alcoz J J, Gibler W, Atkins R A and Taylor H F 1991 Method for embedding optical fibers and optical fiber sensors in metal parts and structures *Proc. SPIE* **1588** 110
[4] Lin Gang-Chih, Wang Likarn, Yang C C, Shih M C and Chuang T J 1998 Thermal performance of metal-clad fiber Bragg grating sensors *IEEE Photon. Technol. Lett.* **10** 406
[5] Baldini S E, Tubbs D J and Stange W A 1990, Embedding fiber optic sensors in titanium matrix composites *Proc. SPIE* **1370** 162
[6] Reid M 1998 Temperature dependence of fiber optic Bragg gratings at low temperature *Opt. Eng.* **37** 237